Space-time-based Detection of Infrared Small Moving Target

Wencheng Wu[1] and Askar Hamdulla[1,*]

[1] *Institute of Information Science and Engineering, Xinjiang University, Urumqi 830046, China*
[*] *Corresponding author. E-mail: askar_H@21cn.com*

Received: May. 15, 2019, Accepted: May. 10, 2020

With the development of infrared monitoring and early warning system, more and more attention has been paid to the research of infrared small target detection. How to effectively detect the target in a complex background has always been a major challenge for researchers. This paper presents a space-time-based detection for small infrared target, which can improve the performance of infrared small target detection system. Firstly, the targets are enhanced and the background clutter is suppressed by the morphological filter. Then, the segmentation images method is proposed to erase the majority noises, which calculates an adaptive thresholds based on the constant false alarm rate (CFAR). Finally, a dynamic detection is proposed to erase all of the noises in the multi-frame, which adjust the size and position of the search window based on the kinematic rule of targets. Experimental results show that this technology can effectively detect the small infrared target with high performance.

Keywords: Morphology filter; Constant false alarm rate CFAR; Motion feature analysis; Point target detection; SNR of point target

http://dx.doi.org/10.6180/jase.202009_23(3).0014

1. Introduction

Affected by the development of stealth technology, the method using radar and other electromagnetic equipment to locate and track targets is gradually unfit the demand of the contemporary military. Because current weapons have high thermal radiation, the technologies of infrared small target detection have been paid attention to in many fields, such as monitoring systems, early warning systems, and target tracking systems. To meet the ability of rapid warning, this system is far away from the target [1, 2]. Due to the long-distance and atmospheric transmission effect, the targets are usually tiny and dim, with no texture, which easily submerged by background and noise [3]. Those factors make the detection and tracking of small infrared targets more difficult [4]. Therefore, how to efficiently and accurately detect moving infrared small targets under low signal-to-clutter ratio (SNR) has been extensively studied in the field of Automatic Target Recognition (ATR) in recent years.

In the past few decades, researchers have proposed a large number of algorithms for small target detection [5, 6]. Generally, Infrared small targets appear in the Gaussian form in the image, which is the foundation to distinguish target and background clutter. The single-frame-based detection algorithms analysis the pixels difference between target and background clutter [7, 8]. The traditional methods detect target by background estimation, such as median filtering, maximum mean filtering and maximum median filtering [9]. They detect the small infrared target by subtracting the estimated background from the original image. Max-median/Max-mean filters can suppress noise and background clutter to some extent, but those methods are more or less time-consuming [10]. Top-Hat transform algorithms based on contour structure morphology enhance target by background clutter suppression [11]. It is fast enough, but it can not adapt to different environments. New Top-hat improves the robustness of the algorithm by changing the structuring elements to suppress the effect of noises is a direct way to improve the performance of top-hat transformation [12]. However, when the SNR is lower, the false alarm still increases. Zhang et al. proposed a small target detection algorithm based on difference, clustering and Gaussian curvature [13]. By analyzing the difference between target and noise, the pixel is eliminated as the non-uniform region through clustering, and then the target was extracted with Gaussian curvature. Yang et al. [14, 15] proposed an eight-direction and three-layer window and fuzzy-theory-based adaptive parameters to enhance the robustness of the system. The multi-frame-based algorithms detect small infrared moving targets in a sequence of images [16, 17]. By analyzing the kinematic rule of targets, those algorithms erase noise, preferably [18].

To pursue a better performance, this paper proposes a detection of small infrared moving targets by combining time and space. Firstly, the targets are enhanced and the background clutter is suppressed by the morphological filter. Then, an adaptive thresholds image segmentation based on the constant false alarm rate (CFAR) [19] is used to erase the majority noises. Finally, a dynamic detection based on the kinematic rule of targets is proposed to erase all of the noises in the multi-frame. The experimental results and analysis show that the proposed method can detect small infrared targets with high detection rate, low false alarm under the interference of strong noise and complex backgrounds.

This paper is organized as follows. Section 2 discusses the detailed elaboration about the small infrared target detection method based on combining time and space. Section 3 shows the experimental results and analysis. Finally, Section 4 summarizes the main work of this paper.

The main work and contribution of the thesis as follows: Firstly, it analyzes the defects of the small infrared target detection based on morphological filter. Then it proposes an image segmentation algorithm to erase the majority of noises, which calculate the adaptive segmentation threshold by CFAR. Secondly, it proposes the dynamic detection algorithm to erase the target-like noises, which proposes a new dynamic search strategy with adaptive search window by analyzing the kinematic rule of targets.

2. Infrared weak point target detection

In the algorithm mentioned in this paper, the preprocessing of images before multi-frame detection is essential and is an integral part of ensuring the real-time performance of the system. The purpose of preprocessing is to remove the background as much as possible. In this paper, the effect of pretreatment is evaluated by the SNR (signal to noise ratio). The model of the point target takes the form:

$$I(i,j) = \begin{cases} T(i,j) + B(i,j) + N(i,j) & \text{Existing target} \\ B(i,j) + N(i,j) & \text{No target} \end{cases} \tag{1}$$

where $T(i,j)$ is the pixel of the target. $B(i,j)$ is the pixel of the background. $N(i,j)$ is the pixel of the zero mean and variance as σ^2 Gaussian distribution noise, which takes the form:

$$\frac{1}{n}\sum_{(i,j)} N(i,j)^2 = \frac{1}{n}\sum_{(i,j)} \left(p_{(i,j)} - \mu\right)^2 = \sigma^2 \tag{2}$$

where the $p(i,j)$ is the pixel in image, μ is the mean of image pixels The SNR Theorem states that the image SNR is the ratio of power spectrum of the noise and signal. It be converted to dB as follow:

$$SNR_1 = \log_{10}\frac{(T-B)^2}{\sigma^2} \tag{3}$$

where T is the power of target, B is the estimated of background's power, and it is estimated by the average of every pixel in the image. σ^2 is the estimated of noise's power, and it is estimated from the pixel-based histogram analysis.

To calculate the SNR of the image after preprocessing, the pixel of the background has been suppressed, this means, it doesn't consider $B(i,j)$ within the target model. Therefore, the SNR of the image after preprocessing takes the form:

$$SNR_2 = \log_{10}\frac{T^2}{\sigma^2} \tag{4}$$

In the aspect of the pretreatment, this paper contains two procedure: morphology filter-based target enhancement and CFAR-based automatic image threshold.

2.1. Morphological filtering

Given the dot appearance target in the infrared image, we suppresses the clutter and background to enhance the target by preprocess by the morphological filtering. It takes the form:

$$\begin{cases} \delta_{\text{expansion}} = f_{\text{ing}} \square D \\ \delta_{\text{corrosion}} = f_{\text{ing}} \square \in E \\ f_{\text{img}}{}' = \delta_{\text{expansion}} - \delta_{\text{corrosion}} \end{cases} \tag{5}$$

Here, we have define f_{img}, represents the original image. The $\delta_{\text{expansion}}$ and $\delta_{\text{corrosion}}$ are the images after expansion and corrosion with original image using the kernel D and E. They have achieved effects of clutter suppression and target enhancement, respectively. And $f_{img'}$ represents the image after target-enhanced and background and clutter-suppressed, which can be calculated by subtracting δ_{expamion} from $\delta_{\text{corrosion}}$. The size of D and E is 5. Fig. 1 shows the images of $\delta_{\text{expansion}}$, $\delta_{\text{corrosion}}$ and f_{img}. Specifically, Fig.1 (a) show the original image. Fig.1 (b) is the dilation image from original image, which target is enhanced, obviously. Fig.1 (c) is the erosion image from original image, which clutter is suppressed, obviously. And

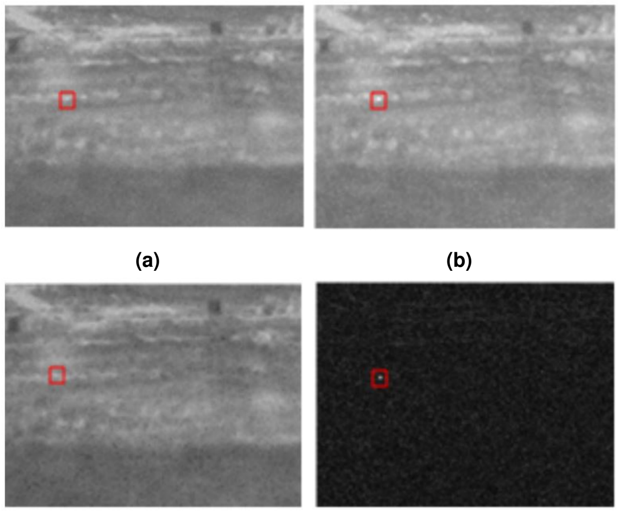

(a) (b)

(c) (d)

Fig. 1. Example of target enhancement by morphological filtering of a base sample. (a) Original image. (b) $\delta_{\text{expansion}}$. (c) $\delta_{\text{corrosion}}$. (d) $f_{\text{ing}'}$.

Fig.1 (d) is the top-hat image from original image, which background is suppressed, obviously.

In order to verify the algorithm's feasibility of the dim target enhancement in infrared image, we calculate the SNR of both original image and $f_{\text{ing}'}$, by passing through the above Eq. 3, respectively.

Fig. 2 shows the grey statistics histogram of original image and $f_{\text{ing}'}$. Furthermore, through Gaussian fitting, the average grey value u and σ^2 is calculated. Gaussian takes the form:

$$G(x) = \frac{1}{\sqrt{2\pi\sigma}} \exp\left(-\frac{(x-u)^2}{2\sigma^2}\right) \tag{6}$$

Then, according to the fitting curve by MATLAB, the coefficient of Gaussian is calculated. Therefore, u_1 and σ_1^2 of the original image are 131.1 and 30.29 , respectively. u_2 and σ_2^2 of the f_{ing} , are 24.92 and 10.32, respectively.

The SNR of both original image and f_{ing} can be calculated as:

$$SNR_{\text{orginal - inngge}} = \log_{10}\frac{(T-u_1)^2}{\sigma_1^2} = \log_{10}\frac{(250-131.1)^2}{30.29^2} = 1.187 \tag{7}$$

$$SNR_{\text{fret}} = \log_{10}\frac{(T-u_2)^2}{\sigma_2^2} = \log_{10}\frac{(250-24.92)^2}{10.32^2} = 2.68 \tag{8}$$

Figure 1, Eq. 7 and Eq. 8 shows that morphology filter is able to enhance the dim small target in the complex background and image SNR efficiently. Furthermore, we calculate the SNR of 200 images of the original image and

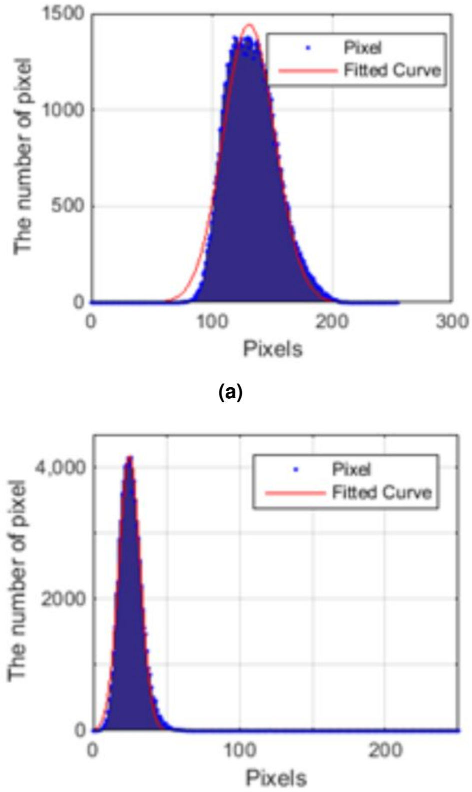

(a)

(b)

Fig. 2. Gray histogram and Gaussian fitting both of image pixels. (a) From the o1riginal image. (b) From the $f_{ing'}$.

$f_{ing'}$, respectively. It can be seen that the SNR of the preprocessed image is always higher than that of the original image.

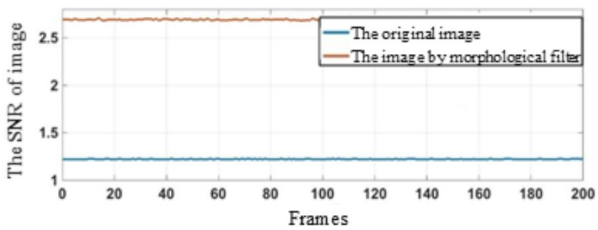

Fig. 3. The SNR of 200 images of the original image and $f_{ing'}$, respectively.

2.2. Image segmentation based on CFAR

Though the series of morphological operation in the original image, background and clutter can be suppressed to some extent. But there is still background noise (see Figure 1d). We need an adaptive threshold to segment the image so that there are only target pixels as possible in the image.

Here the threshold T must the following requirements:

$$f(x,y) = \begin{cases} 0 & f_{img'} < T \\ f_{img'} & f_{img'} \geq T \end{cases} \tag{9}$$

The constant false alarm rate (CFAR) processing of radar signal is an important item of modern radar signal processing. CFAR detection refers to a common form of adaptive algorithm used in radar systems to detect target returns against a background of noise, clutter and interference. The role of the CFAR circuitry is to determine the power threshold above which any return can be considered to probably originate from a target. If this threshold is too low, then more targets will be detected at the expense of increased numbers of false alarms. Conversely, if the threshold is too high, then fewer targets will be detected, but the number of false alarms will also be low. The threshold provides a specified probability of false alarm, governed by the probability density function of the noise, which is usually assumed to be Gaussian. The probability of detection is then a function of the signal-to-noise ratio of the target return.

The processing environment of infrared point target is similar to that of radar signal, we use CFAR to calculate the T. The CFAR algorithm takes three parameters: false alarm probability P_f, probability density function of the noise and probability density function parameter. We introduce the histogram approximation method to determine and verify the model of probability density function of the noise. The noise in $f_{ing'}$ is subject to Gaussian distribution, which is provided in Figure 2(b).

Figure 4 shows that CFAR work to calculate the threshold $T.f(x)$ is the probability density function of the noise, $s(x)$ is the probability density function of the target. The hatched section P_f shows the false alarm probability, which takes form:

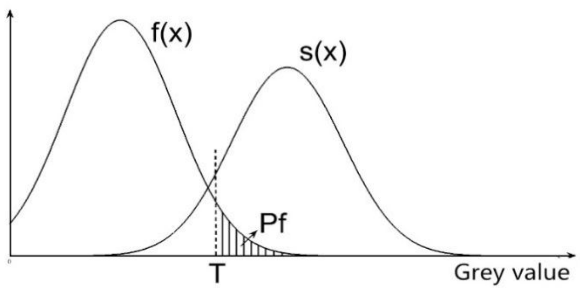

Fig. 4. CFAR work to calculate the threshold T.

$$P_f = \int_T^{+\infty} f(x) d_x = \int_T^{+\infty} \frac{1}{\sqrt{2\pi\sigma^2}} e^{-\frac{(x-\mu)^2}{2\sigma^2}} d_x \tag{10}$$

On account of the primitive of Gaussian distribution can't be expressed exactly, we depict approximately the primitive through the Gauss error function $\text{exf}(x)$. The Eq. 10 can rewrite as:

$$\begin{aligned} P_f &\approx \tfrac{1}{2}\sqrt{-\tfrac{x-\mu}{\pi}}\,\text{erf}\,i(\sqrt{-\tfrac{(x-\mu)^2}{2\sigma^2}}) \\ &\approx \tfrac{1}{2}\sqrt{-\tfrac{x-\mu}{\pi}}\,\tfrac{2}{\sqrt{\pi}} e^{-\frac{(x-\mu)^2}{2\sigma^2}} D(\sqrt{-\tfrac{(x-\mu)^2}{2\sigma^2}}) \end{aligned} \tag{11}$$

where, the $D(z)$ is the Dawson function(which can be used instead of $\text{exff}(z)$ to avoid arithmetic overflow), which takes form:

$$D(x) = e^{-x^2} \int_0^x e^{t^2} dt \tag{12}$$

We calculate approximately the threshold T by fixing P_f of Eq. 11 , which takes the form:

$$T = \mu + E \times \left(1 - P_f^2\right) \times \sigma \tag{13}$$

where σ and μ are the mean and standard deviation of $f(x)$ and E is approximated as $\frac{\pi^2\mu^2}{\sigma^2}$.$P_f$ is related to the number of targets in infrared image, which takes form:

$$P_f = \frac{\text{target} \ - \ \text{number}}{\text{all number}} \leq 10^{-4} \tag{14}$$

To improve the performance of CFAR algorithm, P_f is set as less than 10^{-4}. In fact, the all number is known as the image size. That means that the target. number should be confined to a certain extent. In this paper, all. number is $76800(240 \times 320)$ in one example, and the target. number is less than 7. Here, target number is assumed as 5, then $P_f = 6.5 \times 10^{-5}$

Figure 5 shows the result of CFAR image segmentation, there are four points in the image, among which there is only one target, the rest are the noise similar to target. Figure 6 shows the process flowchart of the preprocessing

2.3. Motion based Target detection

This preprocessing suppress effectively the background and clutter, but the pre-processed image still has false alarm, when there are some noise that is similar to target(as show in Figure 5). At low SNR, it is hard thing to accurately detect the target just in one infrared image. However, the target has kinematic rule in a short time in the video, its kinematic rule is assumed with uniform straight line motion, and the pixels of target is sequential similarity in adjacent frame. This paper proposes the dynamic methods, which employ the kinematic rule and sequential similarity of real target to erase ghosts. Here, the target's motion model takes form:

$$\begin{aligned} &F(x,y,t) = ax_t + y_t \\ &g(x,y,t) \approx g(x',y',t+1) \end{aligned} \tag{15}$$

where (x,y,t) represent the target position in the image at time $t.a$ represent the target moving direction, that is calculate by adjacent frame. $g(x,y,t)$ represent pixel at

(a)

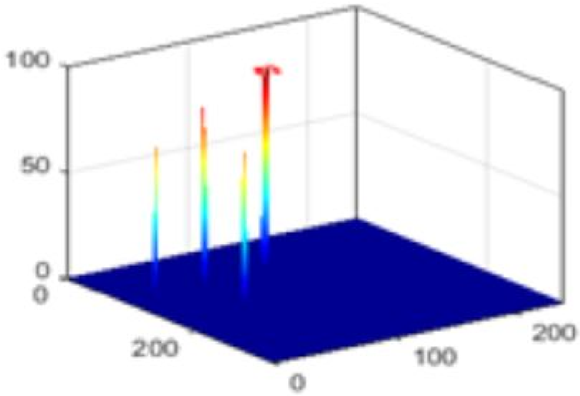

(b)

Fig. 5. The result of CFAR image segmentation. (a) The image from the segmentation. (b) The 3D mesh of (a).

(x, y) at time t. Dynamic methods based infrared target detection mainly divides into the following several steps:

A) Calculate the target moving direction by adjacent frame.

B) Select the search, though motion model, to find the most correlative results in the next frame. Erase ghosts when the correlation that does not exist between two adjacent frame in the video.

C) Update the target moving direction and the experience standard deviation.

2.3.1. Motion model

Figure 7 shows the process that calculate target moving direction between the first frame and the second frame, both of them are preprocessed by CFAR. In the second frame, the targets are searched on the 2 -adjacent areas of the positions (the black of Figure 7) that correspond to the targets which are detected in the first frame. The target moving directions a (the blue line of Figure 7) are calculate when there are suspicious targets that is similar to the target in the first frame (the grey of Figure 7) on the search area. Here, the a can be formulated as follows:

$$\mathrm{a} = \frac{y_t - y_{t-1}}{x_t - x_{t-1}} \tag{16}$$

where x and y is the position of the pixel in image.

The search area is selected (the red boxes of Figure 8) in the third through the target moving direction that is determined before. If there are suspicious targets in the search area and which is correlative with targets of adjacent frame, it is reserved as targets (the 4^{th} red box of Figure 8). If there are suspicious targets in the search area but which is not correlative with targets of adjacent frame, the suspicious target and this target moving direction is erased as noise (the 3^{th} red box of Figure 8). If there are not suspicious targets in the search area, this target moving direction is erased as noise (the 1^{th} and the 2^{th} red box of Figure 8). Figure 8 shows the dynamic detection method filter out the noise effectively (the 1^{th} , the 2^{th} and the 3^{th} gray block of Figure 8, and the 1^{th} and the 2^{th} blue block of Figure 8). Meanwhile, the dynamic detection method accumulates the energy in the multi-frame images along the target trajectories, the target moving direction and the correlation template are more accurate with time going on, then chooses a target trajectory whose accumulation value is biggest from all possible trajectories.

The correlation discriminant is takes form:

$$\text{target}_{\text{piral}} \in \{\mu_p - \alpha_p, \mu_p + \alpha_p\} \tag{17}$$

where μ_p and α_p are mean and standard deviation of targets in 5 -adjacent frames. target $_{\text{prat}}$ represent the pixel of suspicious targets in current frame.

In order to improve the algorithms' performances in long-term working, the targets moving direction a need to be updated during deviation. Equation 15 can be rewritten as follows:

$$a = \frac{1}{n}\left(\frac{y_{t-n} - y_{t-n+1}}{x_{t-n} - x_{t-n+1}} + \cdots + \frac{y_{t-1} - y_t}{x_{t-1} - x_t}\right) \tag{18}$$

where, n is related to the target's movement speed. After direction is determined, the default size of search area is triple of target (the red dotted box of the Figure 9). Meanwhile, here n is set to 6 by default. The size of search area doubled adaptively, when there is no suspicious targets in current search area (the red box of the Figure 9). Meanwhile, here n doubled adaptively.

The performance of dynamic detection method is related to the number of frames. As shown in Figure 10, the only one target is detected in the video using 3-adjacent frames and 4-adjacent frames, respectively. When using 3-adjacent frames, there are still false alarm in some frames. When using 4-adjacent frames, there are only still target in

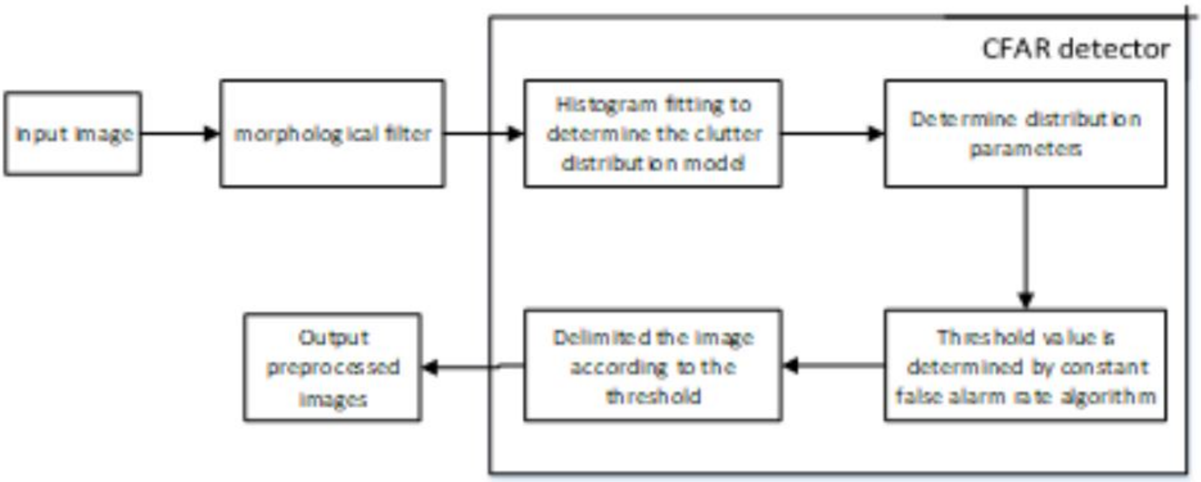

Fig. 6. The process flowchart of the preprocessing.

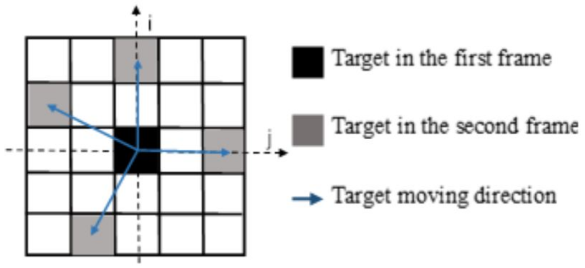

Fig. 7. The process that calculate target moving direction.

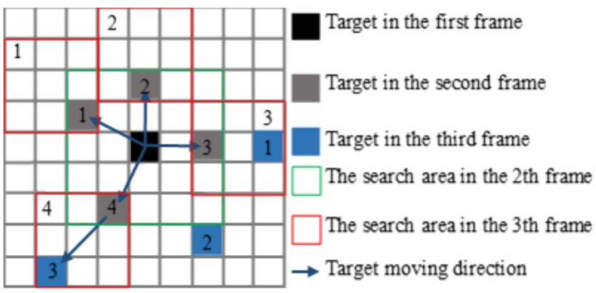

Fig. 8. Dynamic detection method.

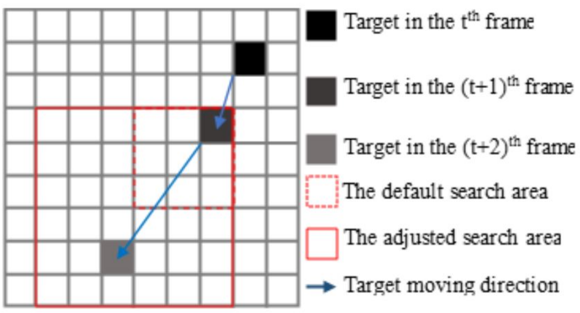

Fig. 9. The adaptive size of search area.

frames. Therefore, the performance of dynamic detection method is improved as we augment the number of adjacent frames.

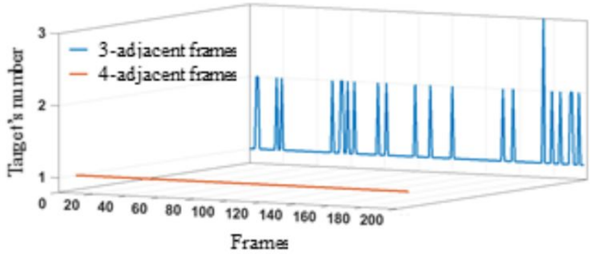

Fig. 10. The dynamic detection' result by using different number of adjacent frames.

Figure 11 shows the target trajectory in 200-frame images (there is only one moving target in the image of Figure 1(a)), which is detected by using 4-adjacent frames. Figure 12 shows the process flowchart of the dynamic detected.

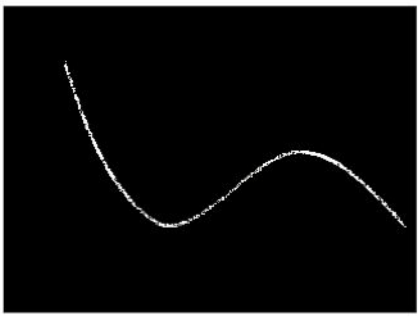

Fig. 11. The target trajectory in 200-frame images*

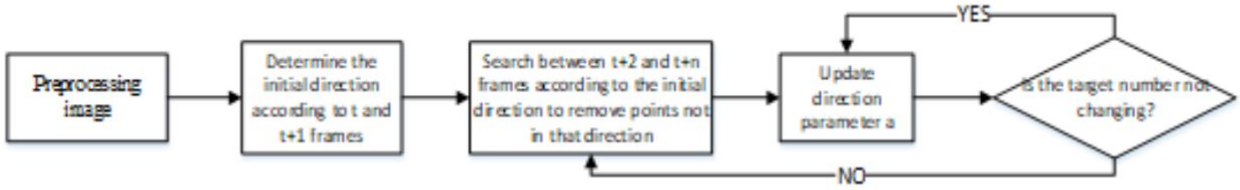

Fig. 12. The process flowchart of the dynamic detected.

Table 1. The details of images.

	Example	3D mesh	Frames	Size	Describe
Seq.1	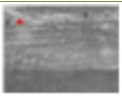	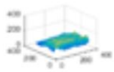	200	320×240	The multi-frame images have only one target with dot clouds, which are added 0 mean and 0.001 variance Gaussian noise on original images.
Seq.2	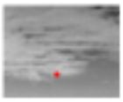	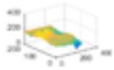	200	320×240	These are added 0 mean and 0.005 variance Gaussian noise on original images.
Seq.3	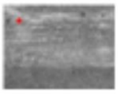	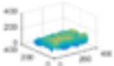	30	256×200	The multi-frame images have only one target with heavy clouds.
Seq.4	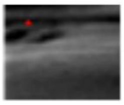	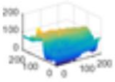	200	250×250	The multi-frame images have only one target with dim background and heavy clouds.

3. Experimental

The performance of the proposed method is evaluated by various experiments. In all experiments, multi-frame infrared images image, including the original image and the additive noise, are used under various complex background. Table 1 shows the details of multi-frame images. These images are captured under different conditions. In Seq.1, there is only one target in the punctiform clouds and clutters. There are 200 frames in this sequence, and the resolution is 320×240 pixels in each frame, which are added 0 mean and 0.001 variance Gaussian noise on original images. The Seq.2 is the images adding 0 mean and 0.005 variance Gaussian noise to original images. In Seq.3, there is one target in heavy clouds. There are 30 frames in this sequence, and the resolution is 256×200 pixels in each frame. The Seq. 4 is the images with dim background and heavy clouds. There are 30 frames in this sequence and there is only one target. The resolution is 250×250 pixels in each frame. Because of the long-distance imaging, the IR small target usually appears as a dim spot masked in the heavy clouds.

3.1. Performance analysis of CFAR in single image

In order to verify algorithm performance, we pre-process the single image that is added 0 mean and 0.001 variance Gaussian noise in original image through CFAR in different environment. The pretreatment experience result and 3D mesh views of six different environment single image as shown in Figure 13. Specifically. Figure 13(a) shows the original images of six different images which include sea environment, sea-airs environment and heavy clouds environment and Figure 13(b) is the 3D mush views of the original images. The six different environment images after morphological filter and their 3D mush views are given in Figure 13(c)-(d), which clearly revealed the morphological filter's performance of target enhancement and background suppression in different environment. The six different environment images after CFAR image segmentation and their 3D mush views are given in Figure 13(e)-(f),

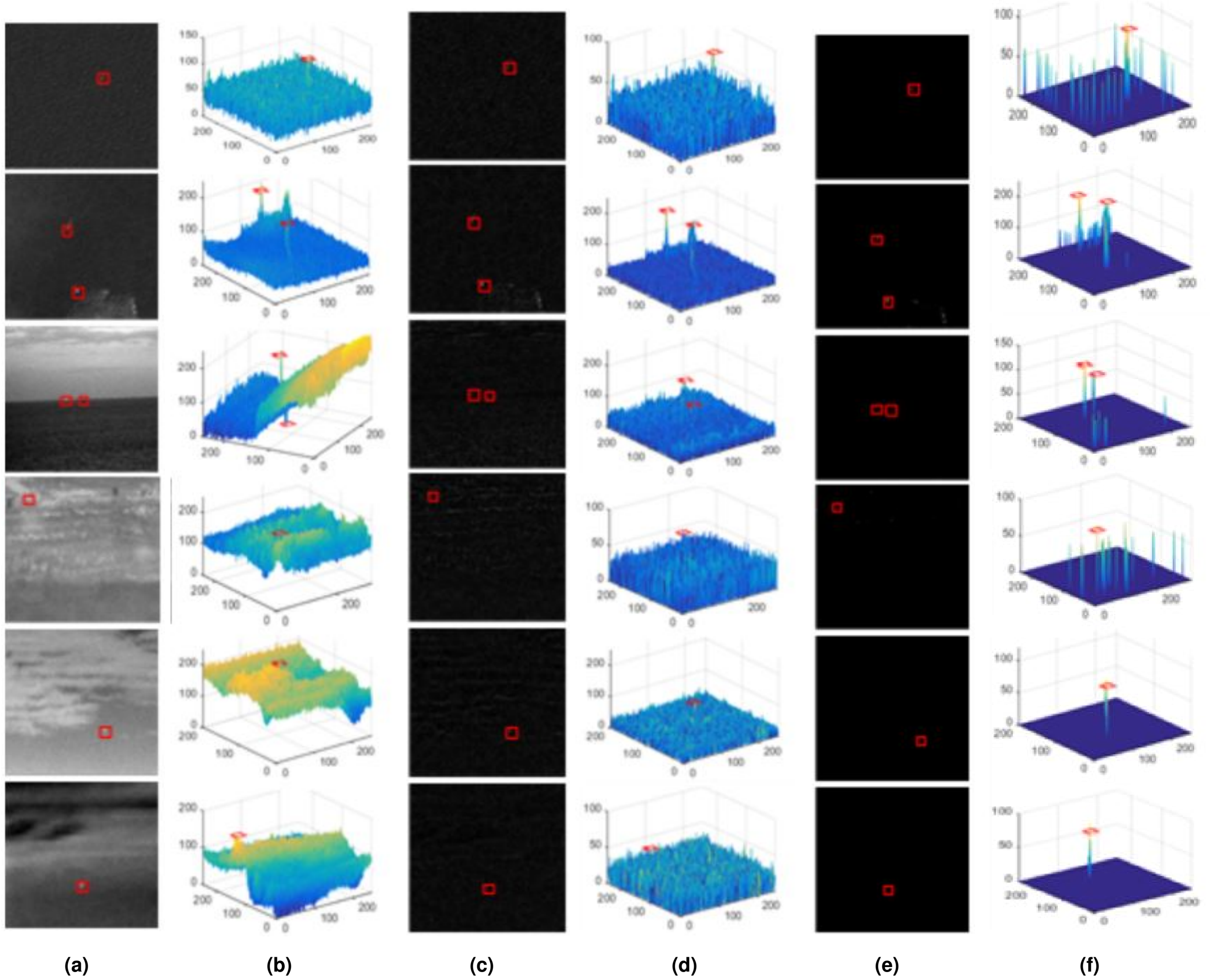

Fig. 13. Original images and pretreatment experimental results of single image in different environment. (a) Original images. (b)The 3D mesh view of original images. (c) The images after morphology filter. (d) The 3D mesh view of images after morphology filter. (e) The images after CFAR segmentation. (f) The 3D mesh view of images after CFAR segmentation.

which clearly revealed the performance of CFAR to erase the background and noise in different environment. Meanwhile, there is only target in the segmented image, when the SNR of the original image is higher (the fifth and the sixth original image of Figure 13). When the SNR of the original image is lower, there are still noises in the image. To a large extent, we can distinguish the target from the background by using the adaptive threshold segmentation

3.2. Analysis of dynamic method in multi-frame

There are noises in the segmented image, when the SNR of original image is lower (the first to the fourth original images of Figure 13). It means that these noises have similar appearance (gray and dot) to targets. So, the he methods of morphological filter based on shape and CFAR image segmentation based on gray cannot erase these noise.

Figure 14 shows the result of Sequence 1(Figure 14(a)), Sequence 2 (Figure 14(b)), Sequence 3(Figure 14(c)) and Sequence 4 (Figure 14(d)) of Table 1 that is processed further by dynamic method after pre-treatment. Figure 14 shows that, in some cases, there are still a few noises when the 3-adjacent frames or 4-adjacent frames are used as a unit in dynamic method in Sequence 1 or when 4-adjacent frames, 5-adjacent frames or 6-adjacent frames are used as a unit in dynamic method in Sequence 2. And in some cases, there are still a few noises when the 1-adjacent frames or 2-adjacent frames are used as a unit in dynamic method in Sequence 3 or in Sequence4. This usually means the target is submerged by noise. Figure 15 shows, on account of images have poor signal to noise ratio (SNR), there only is target when the 5-adjacent frames or 7-adjacent frames are used as a unit in Sequence1 and in Sequence2. And there only is target when the 3-adjacent frames are used as a unit in Sequence 3 and in Sequence 4, on account of images have high signal to noise ratio (SNR). Figure16 shows the target trajectories of sequence 2. The target trajectories is accurate when the 7-adjacent frames are used as a unit in dynamic method.

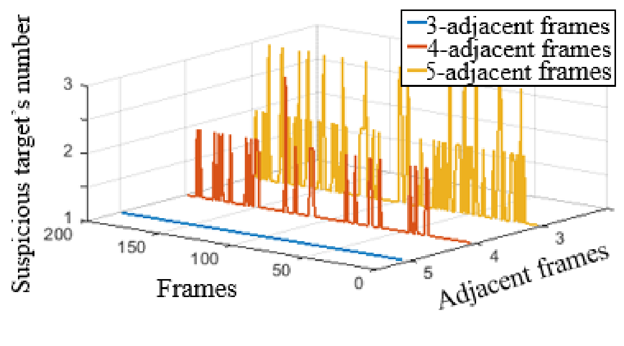

(a)

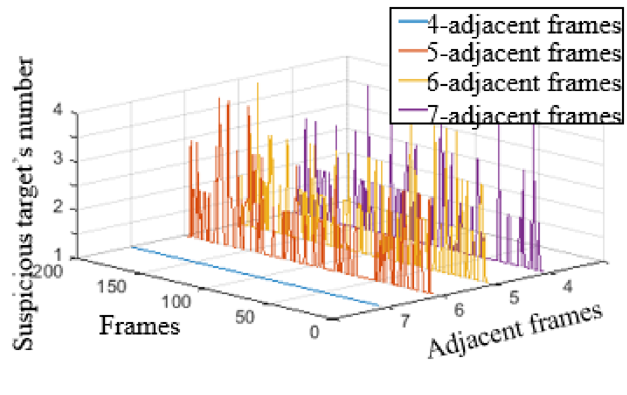

(b)

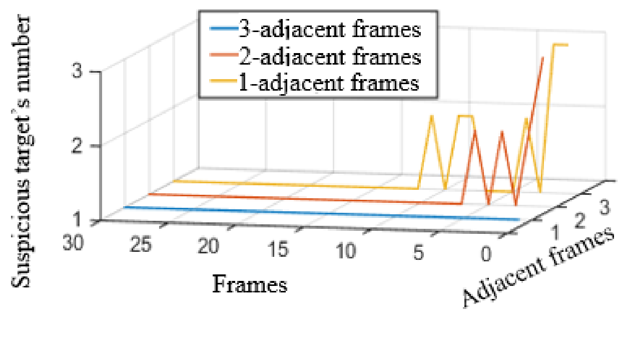

(c)

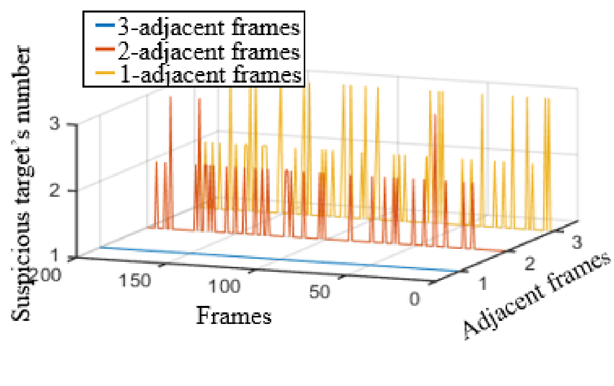

(d)

Fig. 14. The result of Sequence 1, Sequence 2, Sequence 3 and Sequence 4 though dynamic method. (a) Sequence 1. (b) Sequence 2. (c) Sequence 3. (d) Sequence 4.

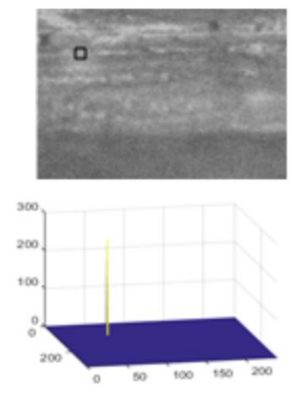

(a)

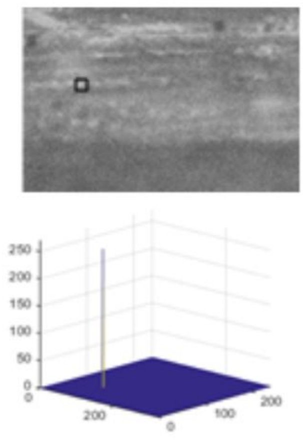

(b)

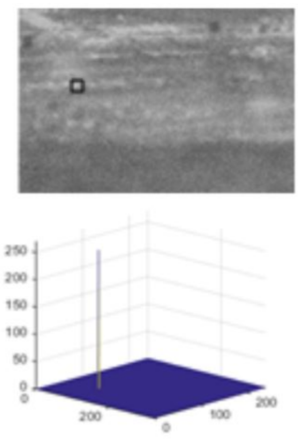

(c)

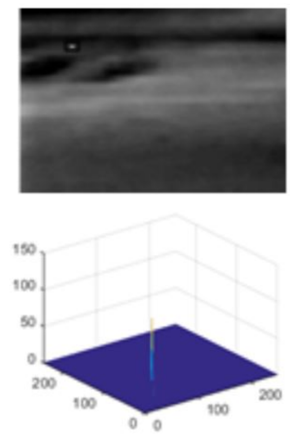

(d)

Fig. 15. The target is submerged by noise. (a) The 17th frame of Sequence 2. (b) The 40th frame of Sequence 2.

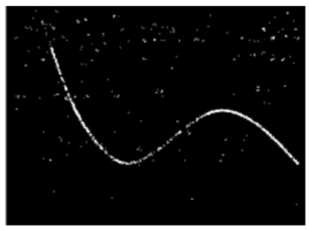

(a)

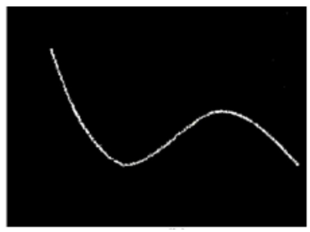

(b)

Fig. 16. The target trajectories of sequence 2, which use 6-adjacent frames and 7-adjacent frames as a unit in the dynamic method. (a) 6-adjacent frames. (b) 7-adjacent frames

3.3. Comparison with other methods

Conventional methods such as Top-Hat, multi-scale local homogeneity measure (MLHM) and Multi-scale Relative Local Contrast Measure (MRLCM) are also performed as comparisons. When the SNR of the Sequence 3's images changes, the ROC curves are plotted in Figure 17. The false alarm is defined in

$$Falsealarm = \frac{\text{number of false pixels detected}}{\text{number of total pix els in im age}} \tag{19}$$

The detection ratio is defined in

$$detectionratio = \frac{\text{number of ture pix els detected}}{\text{number of total true pix els in image}} \tag{20}$$

As Figure 17 shows, the Top-hat [12] and the MLHM [10] detect the target by structure elements that analysis the relationship between target pixels and adjacent pixels, their result is poorer when there are most noises which is similar to target in the images. MRLGMI [20] shows good detection performance but false alarms still exist. The image is segmented by CFAR after Top-hat morphological filter. The false alarm is reduced significantly and the real targets are maintained. Then, the false alarm is reduced by dynamic method further. Our method thus achieves the best detection results. This comparison indicates that dynamic method based on target moving model could better erase the noise which contributes to better detection performance than ordinary methods.

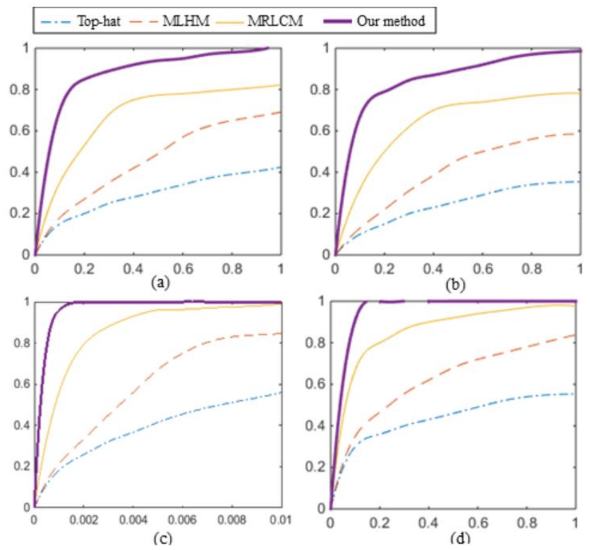

Fig. 17. The ROC curves of four method on the images of the Sequence 1, Sequence 2, Sequence 3 and Sequence 4 with different variance Gaussian noise.

4. Conclusion

In this paper, an infrared small target detection algorithm based on space-time is presented, which improves the accuracy of single-frame-based detection and the efficiency of multi-frame–based detection. The main idea of this method is to enhance the small targets and to suppress background clutter and noise by CFAR and dynamic method. The proposed method mainly utilizes morphological filter and image segmentation erase the background and the majority noises. Further, the suspicious targets are erased by dynamic method which utilize the rule of movement of real target. Furthermore, an adaptive threshold which is calculated by CFAR is adopted to implement targets segmentation. Meanwhile, the infrared image with different SNR in complex background is taken as experimental data. The effectiveness and stability of this method are demonstrated through this infrared images. Finally, experimental results and analysis show the effectiveness and performance of the proposed method.

Acknowledgement

This work has been supported by the National Natural Science Foundation of China (under grant number of 61563049).

References

[1] Bin Wang, Lili Dong, Ming Zhao, and Wenhai Xu. Fast infrared maritime target detection: Binarization via histogram curve transformation. *Infrared Physics and Technology*, 83:32–44, 2017.

[2] Jing Hu, Yi Yu, and Fan Liu. Small and dim target detection by background estimation. *Infrared Physics and Technology*, 73:141–148, 2015.

[3] Changcai Yang, Jiayi Ma, Shengxiang Qi, Jinwen Tian, Sheng Zheng, and Xin Tian. Directional support value of Gaussian transformation for infrared small target detection. *Applied Optics*, 54(9):2255, 2015.

[4] Yujie Li, Huimin Lu, Jianru Li, Xin Li, Yun Li, and Seiichi Serikawa. Underwater image de-scattering and classification by deep neural network. *Computers and Electrical Engineering*, 54:68–77, 2016.

[5] Jinhui Han, Yong Ma, Jun Huang, Xiaoguang Mei, and Jiayi Ma. An Infrared Small Target Detecting Algorithm Based on Human Visual System. *IEEE Geoscience and Remote Sensing Letters*, 13(3):452–456, 2016.

[6] Liu Gang, Wang Fei, and Liu Zhonghua. Infrared aerial small target detection based on digital image processing. *Multimedia Tools and Applications*, 76(19):19809–19823, oct 2017.

[7] Yao Qin and Biao Li. Effective Infrared Small Target Detection Utilizing a Novel Local Contrast Method. *IEEE Geoscience and Remote Sensing Letters*, 13(12):1890–1894, 2016.

[8] Xiaolong Wang and Cuixia Chen. Ship Detection for Complex Background SAR Images Based on a Multiscale Variance Weighted Image Entropy Method. *IEEE Geoscience and Remote Sensing Letters*, 14(2):184–187, 2017.

[9] R. Venkateswarlu. Max-mean and max-median filters for detection of small targets. *Proceedings of SPIE - The International Society for Optical Engineering*, (3809):74–83, 1999.

[10] Jinyan Nie, Shaocheng Qu, Yantao Wei, Liming Zhang, and Lizhen Deng. An infrared small target detection method based on multiscale local homogeneity measure. *Infrared Physics and Technology*, 90:186–194, 2018.

[11] Lizhen Deng, Hu Zhu, Quan Zhou, and Yansheng Li. Adaptive top-hat filter based on quantum genetic algorithm for infrared small target detection. *Multimedia Tools and Applications*, pages 1–13, mar 2017.

[12] Xiangzhi Bai and Fugen Zhou. Analysis of new top-hat transformation and the application for infrared dim small target detection. *Pattern Recognition*, 43(6):2145–2156, 2010.

[13] He Zhang, Yanxiong Niu, and Hao Zhang. Small target detection based on difference accumulation and Gaussian curvature under complex conditions. *Infrared Physics and Technology*, 87:55–64, 2017.

[14] Jinhui Han, Kun Liang, Bo Zhou, Xinying Zhu, Jie Zhao, and Linlin Zhao. Infrared Small Target Detection Utilizing the Multiscale Relative Local Contrast Measure. *IEEE Geoscience and Remote Sensing Letters*, 15(4):612–616, 2018.

[15] Xin Yang, Yanpei Zhou, Dake Zhou, Ruigang Yang, and Yinji Hu. A new infrared small and dim target detection algorithm based on multi-directional composite window. *Infrared Physics and Technology*, 71:402–407, 2015.

[16] Kun Qian, Huixin Zhou, Shenghui Rong, Bingjian Wang, and Kuanhong Cheng. Infrared dim-small target tracking via singular value decomposition and improved Kernelized correlation filter. *Infrared Physics and Technology*, 82:18–27, 2017.

[17] Xiaoliang Sun, Xiaolin Liu, Zhixuan Tang, Gucan Long, and Qifeng Yu. Real-time visual enhancement for infrared small dim targets in video. *Infrared Physics and Technology*, 83:217–226, 2017.

[18] Mahdi Nasiri and Saeed Chehresa. Infrared small target enhancement based on variance difference. *Infrared Physics and Technology*, 82:107–119, 2017.

[19] K Yu, Z Shi, X Lu Selected Papers of the Chinese Society For, and Undefined 2017. Infrared small target detection method based on local threshold attenuation of constant false alarm. *Society of Photo-Optical Instrumentation Engineers Conference Series*, 2017.

[20] Jinhui Han, Kun Liang, Bo Zhou, Xinying Zhu, Jie Zhao, and Linlin Zhao. Infrared Small Target Detection Utilizing the Multiscale Relative Local Contrast Measure. *IEEE Geoscience and Remote Sensing Letters*, 15(4):612–616, 2018.